Stochastic response determination and optimization of a class of nonlinear electromechanical energy harvesters: A Wiener path integral approach

Ioannis Petromichelakis[a], Apostolos F. Psaros[a], Ioannis A. Kougioumtzoglou[a,*]

[a]*Department of Civil Engineering and Engineering Mechanics, Columbia University, 500 W 120th St, New York, NY 10027, United States*

Abstract

A methodology based on the Wiener path integral technique (WPI) is developed for stochastic response determination and optimization of a class of nonlinear electromechanical energy harvesters. To this aim, first, the WPI technique is extended to address the particular form of the coupled electromechanical governing equations, which possess a singular diffusion matrix. Specifically, a constrained variational problem is formulated and solved for determining the joint response probability density function (PDF) of the nonlinear energy harvesters. This is done either by resorting to a Lagrange multipliers approach, or by utilizing the nullspace of the constraint equation. Next, the herein extended WPI technique is coupled with an appropriate optimization algorithm for determining optimal energy harvester parameters. It is shown that due to the relatively high accuracy exhibited in determining the joint response PDF, the WPI technique is particularly well-suited for constrained optimization problems, where the constraint refers to low probability events (e.g. probabilities of failure). In this regard, the WPI technique outperforms significantly an alternative statistical linearization solution treatment commonly utilized in the literature, which fails to capture even basic features of the response PDF. This inadequacy of statistical linearization becomes even more prevalent in cases of

*Corresponding author
Email address: ikougioum@columbia.edu (Ioannis A. Kougioumtzoglou)

nonlinear harvesters with asymmetric potentials, where the response PDF deviates significantly from the Gaussian. Several numerical examples are included, while comparisons with pertinent Monte Carlo simulation data demonstrate the robustness and reliability of the methodology.

Keywords: energy harvesting; path integral; stochastic dynamics; nonlinear system; optimization

---

1. Introduction

Vibratory energy harvesters [1–3] have flourished in recent years as an alternative to common energy sources such as batteries. The rationale behind energy harvesters is that compact and scalable electronic devices, such as wireless sensors [4, 5] and medical implants [6], are designed to function even with very low (sub-milliwatt) power levels. In this regard, energy harvesters aim at converting any available ambient energy into electricity, and eventually powering and enabling the autonomous operation of such devices. In general, energy harvesters exploit the ability of active materials (e.g. piezoelectric) and electromechanical coupling mechanisms to generate an electric potential in response to external excitations. A cantilever beam with piezoelectric patches attached near its clamped end is one of the most widely used energy harvesters [3]. The beam is subjected to environmental excitation causing large strains near the clamped end, thus producing a voltage difference across the patches. Utilizing an appropriate circuit, the electric potential is converted into current; therefore, mechanical energy is transformed into electrical.

Typically, energy harvesters have been modeled in the literature as linear systems. In this regard, they have been designed (e.g. by tuning the first modal frequency of the beam) to achieve resonance with a given a priori known deterministic (harmonic) excitation, and therefore maximize the energy output [7, 8]. Of course, any kind of deviation of the excitation from its pre-assumed harmonic nature decreases the resonance phenomenon, and reduces the efficiency and energy output of the energy harvester. Thus, to increase robustness

and the coupling range between the excitation and the harvester, researchers intentionally introduced nonlinearities to the design of the energy harvester [9], (e.g., via utilizing magnetic forces) resulting in a nonlinear restoring force. For instance, in many applications the restoring force is proportional to the cube of the deflection and such nonlinearities are well known to increase the effective resonance bandwidth of the harvester, allowing for more efficient energy transduction [3]. Further, most energy harvesters operate in tandem with structures and civil infrastructure systems (e.g. bridges), which are subjected to environmental excitations that have random and even time-varying characteristics. Thus, researchers have recently realized the need for modeling the excitations as stochastic processes [10–14].

Obviously, the ultimate goal is to design and optimize an energy harvester for maximizing its energy output. The analysis and optimization of most harvesters has been done by relying on steady-state analyses under deterministic harmonic excitations [15]. Further, the few papers that consider stochastic excitations almost exclusively utilize the maximization of the average (mean) harvested power as the optimization criterion [16–18]. However, the suitability of alternative performance measures was discussed in [19], and the need for considering higher-order or peak energy (or voltage) statistics in the optimization process was highlighted. In particular, knowledge of the voltage peak statistics, or the probability the voltage remains above a certain level, could be used to safeguard associated electronic circuits, or for an enhanced utilization of the capacitors, respectively. Furthermore, additional restrictions in terms of maximum displacement of the mechanical oscillator may be required in realistic situations due to limited available space, or to avoid potential mechanical failures. In this regard, constraints may often relate to the probability that the voltage and/or the displacement stay within prescribed limits. Overall, incorporation of such "extreme values" statistics as objectives and constraints in the energy harvester optimization problem can lead, potentially, to a more robust and efficient design than what is currently the norm in the literature. A requirement for this, however, is the complete stochastic characterization of the system response, i.e.,

knowledge of the joint response transition probability density function (PDF), and not only of the response mean and standard deviation. Thus, the standard statistical linearization technique [20], which relies on a Gaussian response assumption and has been widely employed to analyze and optimize such energy harvesting systems [18, 21, 22], cannot possibly be used when low probability events enter the optimization problem as requirements and constraints.

In this paper, a methodology for stochastic response determination and optimization of nonlinear energy harvesters is developed based on the Wiener path integral technique (WPI) [23–26, 26, 27]. To this aim, first, the WPI technique is extended to account for the singular diffusion matrix related to the governing equations. In this regard, the electrical equation is construed as a constraint, leading to a constrained variational problem to be solved either by Lagrange multipliers [28], or by nullspace [29] based approaches. Next, the herein extended WPI technique, which exhibits significant accuracy in determining the joint response PDF, is coupled with an appropriate optimization algorithm for determining efficiently the optimal parameters of the energy harvester. Several numerical examples are included, while comparisons with pertinent Monte Carlo simulation (MCS) data demonstrate the reliability and robustness of the methodology. It is shown that, especially for optimization problems with constraints referring to low probability events, the WPI technique outperforms the standard statistical linearization, which fails to capture basic features of the non-Gaussian response PDF, and in many cases violates the constraints.

2. Nonlinear electromechanical energy harvester

2.1. Modeling aspects

One of the most widely studied electromechanical energy harvesters is a cantilever beam with piezoelectric patches attached near its clamped ends. As discussed in detail in [3], the dynamics of such a system can be approximated by the following general mathematical model of coupled electromechanical equa-

tions, expressed in a non-dimensional form as

$$\ddot{x} + 2\zeta\dot{x} + \frac{dU(x)}{dx} + \kappa^2 y = w(t) \tag{1a}$$

$$\dot{y} + \alpha y - \dot{x} = 0 \tag{1b}$$

where x denotes the response displacement and y represents the induced voltage in capacitative harvesters or the induced current in inductive ones. Further, ζ is the damping, κ is the coupling coefficient, α (referred to as the electrical constant in the following) is defined as the ratio between the mechanical and electrical time constants of the harvester (see [21]), and $U(x)$ denotes the potential function. Its derivative $\frac{dU(x)}{dx}$ represents the restoring force, which is nonlinear in general; see [3] for more details. Also, $w(t)$ represents the external excitation, which is modeled as a Gaussian white noise stochastic process. Details regarding the non-dimensionalization of the governing equations can be found in [21] and [30].

In modeling the restoring force $\frac{dU(x)}{dx}$, a wide range of nonlinear behaviors can be captured by the 3^{rd} order polynomial

$$\frac{dU(x)}{dx} = x + \lambda x^2 + \delta x^3 \tag{2}$$

where λ and δ control the intensity of the quadratic and cubic nonlinear terms, respectively, while the coefficient corresponding to the linear stiffness term is 1 as a result of the non-dimensionalization [21]. Further, considering the behavior of the potential function $U(x)$ that controls the essential dynamics of the system, for $\delta \geq 0$, Eq. (2) leads to a bistable asymmetric potential for $\lambda > 2\sqrt{\delta}$, to a monostable asymmetric for $\lambda \leq 2\sqrt{\delta}$, and to monostable symmetric for $\lambda = 0$. As shown in [21], for $\lambda = 0$ and Gaussian white noise excitation, the maximum mean harvested power is achieved for $\delta = 0$, or in other words, the linear system is optimum; see also [31–34] for a relevant discussion on the optimality of linear systems under certain conditions. Furthermore, references [22] and [30] demonstrated that utilizing nonlinear oscillators with symmetric bistable potentials, i.e., $\lambda = 0$ and a restoring force of the form $\frac{dU(x)}{dx} = -x + \delta x^3$, can be beneficial for maximizing the mean harvested power. In this regard, a question

is posed naturally regarding the performance, in terms of harvesting efficiency, of potential functions with asymmetries, i.e., $\lambda \neq 0$. This was addressed by He and Daqaq [21], who studied monostable harvesters in the regime $0 \leq \lambda \leq 2\sqrt{\delta}$, and determined their response statistics by employing a statistical linearization approach. It was shown that the maximum mean harvested power is achieved for some $\delta > 0$ and for the bistability limit $\lambda = 2\sqrt{\delta}$.

In this paper, without loss of generality and taking into account the aforementioned studies, the class of nonlinear energy harvesters with restoring forces given by Eq. (2) with $\lambda = 2\sqrt{\delta}$ and $\delta \geq 0$ is considered. The excitation is modeled as a stationary Gaussian white noise process with a constant power spectrum value S_0, under which, the system response vector process $\boldsymbol{q} = [x, \dot{x}, y]^T$ starts from initial conditions, exhibits a transient phase, and eventually reaches stationarity where the maximum response variance is observed. In this regard, the mean harvested power P_h is proportional to the variance of the zero-mean electrical quantity y and is given by

$$P_h = \alpha \mathbb{E}\{y^2\} \tag{3}$$

where $\mathbb{E}\{.\}$ represents the expectation operator.

2.2. Optimization aspects

From an optimal design perspective, the objective is typically articulated in the literature as maximizing the mean stationary harvested power for a given excitation intensity S_0. This can be formulated as an optimization problem in the set of parameters $\{\zeta, \kappa, \alpha, \delta\} \subseteq \mathbb{R}^4_{++}$, where $\mathbb{R}_{++}$ denotes the set of positive real numbers. The complexity of the problem can be further decreased by investigating the role of each parameter ζ, κ and α in the dynamics of the system.

Specifically, it can be readily seen from equations (1) and (3), that the coupling coefficient κ has a monotonic effect on the harvested power. The strongest the coupling between the mechanical and electrical systems, the largest the variance of the electrical quantity y. As a result, κ should take the largest

value possible, and thus, can be excluded from the optimization problem. The parameter ζ results from the non-dimensionalization of the original equations (e.g. see [3]) and includes the mass, damping and stiffness coefficients of the mechanical system. Therefore, it can be regarded as a scale parameter, which is considered fixed because its value is dictated by physical constraints of the particular application. As a result, it is excluded from the optimization problem as well.

On the other hand, the electrical constant α appears to affect the response quantity y in a more complex manner than κ and ζ. It can be readily seen in Eq. (1) that, for small values of α, $\dot{y}$ approaches $\dot{x}$ and thus, the quantity of interest $\mathbb{E}\{y^2\}$ is controlled essentially by the variance of the mechanical displacement x. Further, for large α, the influence of $\dot{y}$ becomes less significant rendering $\mathbb{E}\{y^2\}$ approximately proportional to the variance of the mechanical velocity $\dot{x}$ [35]. In this regard, α can be construed as a weighting factor, controlling the correlation degree between y and each of the response quantities x and $\dot{x}$. Therefore, it becomes evident that no apparent assumptions about optimal α values can be made. Accordingly, for the parameter vector $\boldsymbol{z} = [\alpha, \delta]$ and for ζ, κ and S_0 fixed, the optimization problem can be formulated as

$$\arg\max_{\boldsymbol{z} \in Z} P_h(\boldsymbol{z}) \tag{4}$$

where $Z \subset \mathbb{R}^2_{++}$ is an effective domain of parameter values.

In practice, it is often desirable to apply additional design criteria that enforce constraints related to the probability that y and/or x stay within prescribed limits. Such a constraint can take the general form $P_f < \epsilon$, where the probability of failure P_f is typically related to an "extreme event" characterized by a low probability of occurrence. For instance, P_f can be defined as the probability that either $|x|$ or $|y|$ exceed some prescribed limit, i.e. $P_f = P(|x| > x_{limit} \text{ or } |y| > y_{limit})$. Taking such an additional design criterion into account, the optimization problem in Eq. (4) needs to be reformulated as

$$\arg\max_{\boldsymbol{z} \in Z} P_h(\boldsymbol{z}) \quad \text{s.t.} \quad P_f(\boldsymbol{z}) \leq \epsilon \tag{5}$$

Note, however, that a requirement for addressing this problem, is the complete stochastic characterization of the system response, i.e., knowledge of the joint response PDF, and not only of the response mean and variance. To this aim, the WPI response determination technique is extended and applied herein for addressing the constrained optimization problem of Eq. (5). It is noted that the problem of Eq. (5) is significantly more complex than the standard unconstrained problem of Eq. (4), which is typically addressed in the literature.

3. Wiener Path integral solution technique overview

3.1. Standard formulation

One of the recently developed promising techniques in stochastic engineering dynamics relates to the concept of the Wiener path integral (WPI) [23]. The technique exhibits not only relatively high accuracy in determining the joint response PDF, but also significant versatility as it can account for multi-degree-of-freedom systems with various nonlinearity types [24], as well as for systems with fractional derivative terms [27]. The essential aspects of the technique are delineated in the present section by considering the general class of n-dimensional randomly excited structural/mechanical systems whose dynamics is described by

$$\boldsymbol{D}[\boldsymbol{q}(t)] = \boldsymbol{w}(t) \tag{6}$$

In Eq. (6), $\boldsymbol{D}[.]$ denotes a nonlinear differential operator, $\boldsymbol{q}$ is the system response, and $\boldsymbol{w}$ is a white noise stochastic excitation vector process with $E[\boldsymbol{w}(t_1)\boldsymbol{w}(t_2)] = \boldsymbol{B}\delta(t_2 - t_1)$; $\delta(.)$ denotes the Dirac delta function and $\boldsymbol{B}$ is a deterministic coefficient matrix given by

$$\boldsymbol{B} = \begin{bmatrix} 2\pi S_0 & \dots & 0 \\ \vdots & \ddots & \vdots \\ 0 & \dots & 2\pi S_0 \end{bmatrix} \tag{7}$$

Next, relying on the mathematical framework of path integrals [36], the

transition PDF $p(\boldsymbol{q}_f, \dot{\boldsymbol{q}}_f, t_f|\boldsymbol{q}_i, \dot{\boldsymbol{q}}_i, t_i)$ can be written as [24]

$$p(\boldsymbol{q}_f, \dot{\boldsymbol{q}}_f, t_f|\boldsymbol{q}_i, \dot{\boldsymbol{q}}_i, t_i) = \int\limits_{\mathcal{C}\{\boldsymbol{q}_i, \dot{\boldsymbol{q}}_i, t_i; \boldsymbol{q}_f, \dot{\boldsymbol{q}}_f, t_f\}} W[\boldsymbol{q}(t)][\mathrm{d}\boldsymbol{q}(t)] \tag{8}$$

with $\{\boldsymbol{q}_i, \dot{\boldsymbol{q}}_i, t_i\}$ denoting the initial state and $\{\boldsymbol{q}_f, \dot{\boldsymbol{q}}_f, t_f\}$ the final state, and $\boldsymbol{q}_i = \boldsymbol{q}(t_i)$, $\boldsymbol{q}_f = \boldsymbol{q}(t_f)$, $\dot{\boldsymbol{q}}_i = \dot{\boldsymbol{q}}(t_i)$ and $\dot{\boldsymbol{q}}_f = \dot{\boldsymbol{q}}(t_f)$. Eq. (8) represents a functional integral over the space of all possible paths $\mathcal{C}\{\boldsymbol{q}_i, \dot{\boldsymbol{q}}_i, t_i; \boldsymbol{q}_f, \dot{\boldsymbol{q}}_f, t_f\}$, $W[\boldsymbol{q}(t)]$ denotes the probability density functional of the stochastic process in the path space and $[\mathrm{d}\boldsymbol{q}(t)]$ is a functional measure. Further, the probability density functional for the stochastic vector process $\boldsymbol{q}(t)$ pertaining to the system of Eq. (6) is defined as (e.g., [24])

$$W[\boldsymbol{q}(t)] = \exp\left(-\int\limits_{t_i}^{t_f} \mathcal{L}\left(\boldsymbol{q}, \dot{\boldsymbol{q}}, \ddot{\boldsymbol{q}}\right) \mathrm{d}t\right) \tag{9}$$

where $\mathcal{L}\left(\boldsymbol{q}, \dot{\boldsymbol{q}}, \ddot{\boldsymbol{q}}\right)$ denotes the Lagrangian functional. As noted previously, considering standard structural dynamical systems yields a differential operator $\boldsymbol{D}[.]$ which contains up to second-order time derivatives of $\boldsymbol{q}$ (inertia term). The corresponding Lagrangian functional is expressed as [24]

$$\mathcal{L}(\boldsymbol{q}, \dot{\boldsymbol{q}}, \ddot{\boldsymbol{q}}) = \frac{1}{2}\boldsymbol{D}[\boldsymbol{q}]^T \boldsymbol{B}^{-1} \boldsymbol{D}[\boldsymbol{q}] \tag{10}$$

Note that Eq. (9) can be loosely interpreted as the probability assigned to each and every possible path starting from $\{\boldsymbol{q}_i, \dot{\boldsymbol{q}}_i, t_i\}$ and ending at $\{\boldsymbol{q}_f, \dot{\boldsymbol{q}}_f, t_f\}$.

Clearly, the largest contribution to the functional integral of Eq. (8) comes from the trajectory $\boldsymbol{q}_c(t)$ for which the integral in the exponential of Eq. (9) (also known as stochastic action) becomes as small as possible; see [36] for instance. According to calculus of variations (e.g., [37],[38]) this trajectory $\boldsymbol{q}_c(t)$ with fixed endpoints satisfies the extremality condition

$$\delta \int_{t_i}^{t_f} \mathcal{L}(\boldsymbol{q}, \dot{\boldsymbol{q}}, \ddot{\boldsymbol{q}}) \mathrm{d}t = 0 \tag{11}$$

which leads to the Euler-Lagrange (E-L) equations

$$\frac{\partial \mathcal{L}}{\partial q_j} - \frac{\partial}{\partial t}\frac{\partial \mathcal{L}}{\partial \dot{q}_j} + \frac{\partial^2}{\partial t^2}\frac{\partial \mathcal{L}}{\partial \ddot{q}_j} = 0, \quad j = 1, ..., n \tag{12}$$

with the set of boundary conditions

$$\begin{aligned} q_j(t_i) &= q_{j,i} \quad \dot{q}_j(t_i) = \dot{q}_{j,i} \\ q_j(t_f) &= q_{j,f} \quad \dot{q}_j(t_f) = \dot{q}_{j,f} \end{aligned} \qquad j = 1, ..., n \tag{13}$$

Next, solving equations (12)-(13) yields the n-dimensional most probable path, $\boldsymbol{q}_c(t)$, and thus, a single point of the system response transition PDF can be determined as [24]

$$p(\boldsymbol{q}_f, \dot{\boldsymbol{q}}_f, t_f | \boldsymbol{q}_i, \dot{\boldsymbol{q}}_i, t_i) \approx C \ \exp\left(- \int_{t_i}^{t_f} L(\boldsymbol{q}_c, \dot{\boldsymbol{q}}_c, \ddot{\boldsymbol{q}}_c) \mathrm{d}t \right) \tag{14}$$

In Eq. (14), the normalization constant C can be computed by utilizing the condition

$$\int_{-\infty}^{\infty} \cdots \int_{-\infty}^{\infty} p(\boldsymbol{q}_f, \dot{\boldsymbol{q}}_f, t_f | \boldsymbol{q}_i, \dot{\boldsymbol{q}}_i, t_i) \mathrm{d}x_{1,f} \mathrm{d}\dot{x}_{1,f} \ldots \mathrm{d}x_{m,f} \mathrm{d}\dot{x}_{m,f} = 1 \tag{15}$$

It can be readily seen by comparing equations (8) and (14) that in the approximation of Eq. (14) only one trajectory, i.e., the most probable path $\boldsymbol{q}_c(t)$, is considered in evaluating the path integral of Eq. (8). Regarding the degree of this approximation, direct comparisons of Eq. (14) with pertinent MCS data related to various engineering dynamical systems [24, 27] have demonstrated satisfactory accuracy; see also [39].

Further, note that instead of directly solving the derived E-L equations (12)-(13), an alternative solution approach can be applied for determining the most probable path $\boldsymbol{q}_c(t)$. Specifically, since $\boldsymbol{q_c}$ is an extremum for the functional

$$\mathcal{J}(\boldsymbol{q}) = \int_{t_i}^{t_f} \mathcal{L}(\boldsymbol{q}, \dot{\boldsymbol{q}}, \ddot{\boldsymbol{q}}) \mathrm{d}t, \tag{16}$$

calculus of variations rules suggest that a direct functional minimization formulation can be applied, which can be readily coupled with a standard Rayleigh-Ritz solution approach (see [26, 27, 40]). In this regard, $\boldsymbol{q}$ is approximated by

$$\hat{\boldsymbol{q}} = \boldsymbol{\psi} + \boldsymbol{R}\boldsymbol{h} \approx \boldsymbol{q}. \tag{17}$$

The function $\boldsymbol{\psi}(t)$ is chosen so that it satisfies the boundary conditions, while the trial functions $\boldsymbol{h}(t) = [h_0, h_1, ..., h_{L-1}]^T$ should vanish at the boundaries, i.e. $\boldsymbol{h}(t_i) = \boldsymbol{h}(t_f) = \boldsymbol{0}$. $\boldsymbol{R} \in \mathbb{R}^{n\times L}$ is a coefficient matrix, where L is the chosen number of trial functions considered. Clearly, there is a wide range of options for the choice of functions $\boldsymbol{\psi}$ and $\boldsymbol{h}$. In the ensuing analysis, the Hermite interpolating polynomials

$$\psi_j(t) = \sum_{k=0}^{3} \alpha_{j,k} t^k \tag{18}$$

are adopted, i.e., $\boldsymbol{\psi} = [\psi_1, \psi_2, ..., \psi_n]^T$, where the $n \times 4$ coefficients $\alpha_{j,k}$ are determined by the $n \times 4$ boundary conditions (13). For the trial functions, the shifted Legendre polynomials given by the recursive formula

$$P_{p+1}(t) = \frac{2p+1}{p+1}\left(\frac{2t - t_i - t_f}{t_f - t_i}\right) P_p(t) - \frac{p}{p+1} P_{p-1}(t), \quad p = 1, 2, ... \tag{19}$$

are employed, which are orthogonal in the interval $[t_i, t_f]$, with $P_0(t) = 1$; and $P_1(t) = (2t - t_i - t_f)/(t_f - t_i)$. The trial functions take the form

$$h_l(t) = (t - t_i)^2 (t - t_f)^2 P_l(t). \tag{20}$$

A practical advantage of the Rayleigh-Ritz method is that the variational problem (functional minimization) degenerates to an ordinary minimization problem of a function that depends on a finite number of variables [38]. Specifically, the functional $\mathcal{J}(\boldsymbol{q})$, dependent on the n functions $\boldsymbol{q}(t)$, is replaced by the function $J(\boldsymbol{R})$, dependent on a finite number of $n \times L$ coefficients $\boldsymbol{R}$. Accordingly, the extremality condition (11) is replaced by

$$\frac{\partial J(\boldsymbol{R})}{\partial \boldsymbol{R}} = \boldsymbol{0} \tag{21}$$

which represents essentially a set of nL nonlinear equations for the unknown coefficients (parameters) $\boldsymbol{R}$. Once solved numerically, the most probable path $\boldsymbol{q_c}$ is determined via Eq. (17).

3.2. Computational aspects

Considering fixed initial conditions $(\boldsymbol{q}_i, \dot{\boldsymbol{q}}_i)$ (i.e., system initially at rest), both approaches, i.e. the E-L equations ((12)-(13)) and the Rayleigh-Ritz so-

lution scheme, yield a single point of the joint response PDF via the solution of a deterministic boundary value problem (BVP). According to a brute-force implementation of the WPI technique, choosing a time instant t_f large enough so that the response has reached stationarity, an effective domain of values is considered for the joint response PDF $p(\boldsymbol{q}_f, \dot{\boldsymbol{q}}_f, t_f | \boldsymbol{q}_i, \dot{\boldsymbol{q}}_i, t_i)$. Next, discretizing the effective domain using N points in each dimension, the joint response PDF values are obtained corresponding to the points of the mesh. Specifically, for an n-DOF system with $2n$ stochastic dimensions (n displacements and n velocities) the number of BVPs to be solved is N^{2n}. It is clear that the computational cost becomes prohibitive for relatively high-dimensional MDOF systems. However, efficient implementations, such as the one developed by Kougioumtzoglou et al. [25], can be utilized in conjunction with the WPI technique. Specifically, employing a polynomial expansion for the joint response PDF yields a number of BVPs to be solved equal to the number of the expansion coefficients. This implementation has been shown to follow approximately a power-law function of the form $\sim (2n)^l/l!$ (where l is the degree of the polynomial), which, depending on the value of n, can be orders of magnitude smaller than N^{2n} [25].

4. Extension of the Wiener path integral technique to account for singular diffusion matrices: A constrained variational problem

Taking into account the form of Eq. (1), it can be readily seen that a straightforward application of Eq. (10) is not possible, as it would lead to a singular matrix $\boldsymbol{B}$. Thus, a modification is required to the WPI technique presented in Sec. 3 to account for the special form of Eq. (1). In this regard, consider Eq. (1a) as an under-determined stochastic differential equation (SDE) with 2 unknowns (x and y), excited by the Gaussian white noise process $w(t)$. For this SDE, the Lagrangian can be expressed as

$$\mathcal{L}(\boldsymbol{q}, \dot{\boldsymbol{q}}, \ddot{\boldsymbol{q}}) = \mathcal{L}(x, y, \dot{x}, \ddot{x}) = \frac{1}{4\pi S_0} \left[\ddot{x} + 2\zeta\dot{x} + x + 2\sqrt{\delta}x^2 + \delta x^3 + \kappa^2 y \right]^2 \quad (22)$$

Clearly, considering Eq. (22) alone is inadequate, as the dynamics described by Eq. (1b) have so far been neglected. To proceed, Eq. (1b) is treated next as a

constraint in the form

$$\phi(\boldsymbol{q}, \dot{\boldsymbol{q}}) = \phi(y, \dot{y}, \dot{x}) = \dot{y} + \alpha y - \dot{x} = 0 \tag{23}$$

Eq. (22) in conjunction with Eq. (23) lead to a constrained variational problem, which is addressed in the following either by Lagrange multipliers [41], or by nullspace [29] based approaches.

4.1. Lagrange multipliers

According to the Lagrange multipliers solution approach [38, 42, 28, 43, 41, 44], the function $\boldsymbol{q}(t)$, for which the functional in Eq. (16) reaches an extremum subject to the constraint of Eq. (23), satisfies the E-L equations corresponding to the functional

$$\mathcal{J}^* = \int_{t_i}^{t_f} \left[\lambda_0 \mathcal{L} + \lambda(t)\phi\right] \mathrm{d}t = \int_{t_i}^{t_f} \mathcal{L}^* \mathrm{d}t, \tag{24}$$

where $\mathcal{L}^* := \lambda_0 \mathcal{L} + \lambda(t)\phi$, and λ_0 and $\lambda(t)$ being appropriately chosen scalar and function multipliers, respectively. The corresponding E-L equations become

$$\frac{\partial \mathcal{L}^*}{\partial x} - \frac{\partial}{\partial t}\frac{\partial \mathcal{L}^*}{\partial \dot{x}} + \frac{\partial^2}{\partial t^2}\frac{\partial \mathcal{L}^*}{\partial \ddot{x}} = 0 \tag{25a}$$

$$\frac{\partial \mathcal{L}^*}{\partial y} - \frac{\partial}{\partial t}\frac{\partial \mathcal{L}^*}{\partial \dot{y}} + \frac{\partial^2}{\partial t^2}\frac{\partial \mathcal{L}^*}{\partial \ddot{y}} = 0 \tag{25b}$$

together with the boundary conditions

$$x(t_i) = x_i, \quad \dot{x}(t_i) = \dot{x}_i, \qquad x(t_f) = x_f, \quad \dot{x}(t_f) = \dot{x}_f \tag{26a}$$

$$y(t_i) = y_i, \quad \dot{y}(t_i) = \dot{x}_i - \alpha y_i, \quad y(t_f) = y_f, \quad \dot{y}(t_f) = \dot{x}_f - \alpha y_f \tag{26b}$$

Clearly, the boundary conditions for $\dot{y}(t)$ in Eq. (26b) cannot be arbitrary, and reflect the constraint relationship of Eq. (23).

The scalar λ_0, multiplying the original Lagrangian $\mathcal{L}$, in Eq. (24) can take the value 0 or 1 [28]. Note that for $\lambda_0 = 0$, the influence of $\mathcal{L}$ is eliminated, and the extremal "most probable path" is determined solely by the constraint equation, without considering the effect of the excitation. This solution is physically non-realizable and falls under the category of abnormal extrema [45, 43, 41].

Thus, the case $\lambda_0 = 1$ is considered in the following, which corresponds to the so-called normal extremal solutions.

In this regard, for $\lambda_0 = 1$, $x(t)$, $y(t)$ and $\lambda(t)$ can be found by solving the two E-L equations (25), in conjunction with the constraint Eq. (23) and with the boundary conditions of Eq. (26). Specifically, employing a state variable representation yields a response vector in the form $[x, \dot{x}, \ddot{x}, x^{(3)}, y, \dot{y}, \ddot{y}, \lambda, \dot{\lambda}]^T$ so that 9 boundary values are required for the solution of the BVP. These are the 8 boundary conditions in Eq. (26) together with an arbitrary [38] initial value $\lambda(0)$. It is noted that since independent boundary conditions are provided for x, $\dot{x}$ and y only, the proposed WPI methodology yields the 3-variate joint PDF $p(x, \dot{x}, y)$. According to Sec. 3.2, applying a brute force approach and choosing a number of $N = 30$ spatial discretization points per dimension, yields $30^3 = 27000$ deterministic BVPs to be solved for determining the response PDF $p(x, \dot{x}, y)$. Alternatively, utilizing a 4^{th} order polynomial expansion for the PDF [25], the number of BVPs to be solved is reduced drastically to only $\binom{3+4}{4} = 35$; thus, rendering the WPI technique computationally efficient.

4.2. Nullspace of constraint equations

An alternative solution approach, which takes advantage of the linearity of the constraint Eq. (23) in terms of the variables $\dot{x}$, y and $\dot{y}$, is delineated next. In this regard, adopting the Rayleigh-Ritz scheme of Sec. 3, and utilizing the polynomial expansion $\hat{\boldsymbol{q}} = \boldsymbol{\psi} + \boldsymbol{R}\boldsymbol{h}$ for $\boldsymbol{q}$ (see Eq. (17)), the optimization problem is restricted within the space of solutions of $\phi(\hat{\boldsymbol{q}}, \dot{\hat{\boldsymbol{q}}}) = \hat{\phi}(t) = 0$.

Specifically, linearity of the constraint equation ensures that $\hat{\phi}(t)$ is a polynomial of degree $L+4$ in t (see equations (17) and (20)), with coefficients linear in the $2L$ unknown expansion parameters $\boldsymbol{R} \in \mathbb{R}^{2\times L}$. Setting these polynomial coefficients equal to zero, yields a set of $L+4$ linear equations with $2L$ unknown variables. Of course, for any well-posed constrained optimization problem, the number of independent constraints is smaller than the dimension of $\boldsymbol{q}$. For the herein concerned problem, this yields $L + 4 < 2L$, which provides the lower bound $L > 4$ for the number L of Legendre polynomials used in the polynomial

expansion. Next, expressing the unknown parameters $\boldsymbol{R} \in \mathbb{R}^{2\times L}$ as a vector $\boldsymbol{u} \in \mathbb{R}^p$, where $p = 2L$, the aforementioned equations are cast as a linear system in the form

$$\boldsymbol{A}\boldsymbol{u} = \boldsymbol{b} \tag{27}$$

where $\boldsymbol{A} \in \mathbb{R}^{s\times p}$, $\boldsymbol{b} \in \mathbb{R}^s$ and $s = L + 4$. This system is underdetermined (since $L > 4$), while $\boldsymbol{A}$ might not have full row rank, i.e., $r_A \leq s$. For instance, dependent rows can appear because some of the coefficients of the polynomials $\hat{\phi}(t)$ set to zero, might be zero anyway, leading to $0 = 0$ equations.

It is now possible to restrict minimization of the objective function $J = J(\boldsymbol{u})$, where $\boldsymbol{u} \in \mathbb{R}^p$, to the set of solutions of Eq. (27) which lie on a lower dimensional space of dimension $p - r_A$. To elaborate further, consider solving one of the r_A independent equations for one unknown component of $\boldsymbol{u}$ and substituting it into the rest $r_A - 1$ equations and into the objective function $J(\boldsymbol{u})$. Repeating this process and eliminating one equation and one unknown at every step, eventually decreases the number of equations to $p - r_A$, while also accounting implicitly for the constraints. More rigorously, the vector space $U \subseteq \mathbb{R}^p$ of solutions of the system $\boldsymbol{A}\boldsymbol{u} = \boldsymbol{0}$, can be fully described with the aid of a basis $\boldsymbol{S} = [\boldsymbol{s}_1\ \boldsymbol{s}_2\ \ldots\ \boldsymbol{s}_{p-r_A}]$ for the *nullspace* of $\boldsymbol{A}$ [46] where $\boldsymbol{S} \in \mathbb{R}^{p\times(p-r_A)}$. In this regard, any element $\boldsymbol{u} \in U$ can be represented by an element $\boldsymbol{v} \in V \subseteq \mathbb{R}^{p-r_A}$ as $\boldsymbol{u} = \boldsymbol{S}\boldsymbol{v}$. Then the vector space $U_b \subseteq \mathbb{R}^p$ of solutions of $\boldsymbol{A}\boldsymbol{u} = \boldsymbol{b}$ can be obtained as an affine transformation of U [47]. More specifically, the solutions $\boldsymbol{u} \in U_b$ of Eq. (27) can be represented as $\boldsymbol{u} = \boldsymbol{S}\boldsymbol{v} + \boldsymbol{u}_p$ where $\boldsymbol{u}_p$ is any particular solution of Eq. (27) [46], [47]; see also [48]. It becomes now possible to cast the original constrained optimization problem

$$\underset{\boldsymbol{u}\in\mathbb{R}^p}{\arg\min}\, J(\boldsymbol{u}) \quad \text{subject to} \quad \boldsymbol{A}\boldsymbol{u} = \boldsymbol{b} \tag{28}$$

into the lower dimensional, unconstrained problem

$$\underset{\boldsymbol{v}\in\mathbb{R}^{p-r_A}}{\arg\min}\, J(\boldsymbol{S}\boldsymbol{v} + \boldsymbol{u}_p) \tag{29}$$

which is solved by applying the optimality conditions

$$\frac{\partial J(\boldsymbol{S}\boldsymbol{v} + \boldsymbol{u}_p)}{\partial \boldsymbol{v}} = \boldsymbol{0} \tag{30}$$

Note that the minimizer $\boldsymbol{u}^*$ of Eq. (28) can be obtained by the minimizer $\boldsymbol{v}^*$ of Eq. (29) as $\boldsymbol{u}^* = \boldsymbol{S}\boldsymbol{v}^* + \boldsymbol{u}_p$. Clearly, solving numerically the reformulated unconstrained problem of Eq. (29) is significantly more efficient computationally than addressing the corresponding constrained problem of Eq. (28) [29]. This becomes particularly beneficial when the approach is integrated with the WPI technique. It is emphasized, of course, that such a treatment is possible due to the linearity of the constraint equations. In a different, more general, case, the Lagrange multipliers solution approach of Sec. 4.1 can be adopted.

5. Numerical Examples

To demonstrate the efficiency and accuracy of the proposed technique for analyzing and optimizing energy harvesting systems, a mono-stable asymmetric harvester ($\lambda = 2\sqrt{\delta}, \delta \geq 0$) described by equations (1),(2) is considered in this section. First, utilizing the herein extended WPI technique of Sec. 4, the stationary joint response PDF $p(x, \dot{x}, y)$ is determined. The corresponding marginal PDFs are compared both with pertinent MCS data, and with PDF estimates based on a statistical linearization treatment [20]. It is shown that due to the Gaussian response assumption, the standard statistical linearization implementation (which has been widely utilized for response analysis of energy harvesters described by Eq. (1) [18, 21, 22]) cannot possibly determine accurately the tails of the response PDFs. Thus, it cannot be used in conjunction with optimization problems such as Eq. (5), where the constraint refers to low probability events. Next, optimal energy harvester designs are obtained by using the aforementioned WPI technique in conjunction with Eq. (3) as the objective function of a global optimization algorithm, constrained via a prescribed probability of failure, as in Eq. (5).

5.1. Energy harvester stochastic response analysis

5.1.1. Linear system

The linear system ($\delta = 0$), for which an exact solution exists (i.e., Gaussian response PDF [11]), is considered first. In this regard, the stationary marginal

response PDFs for $\zeta = 0.1$, $\kappa = 0.65$, $\alpha = 0.8$, $\delta = 0$ and $S_0 = 0.05$ determined via the WPI technique are shown in Fig. 1, and compared with the exact solution. It can be readily seen that the WPI technique exhibits a high degree of accuracy, while there is practically no difference between the results produced by the Rayleigh-Ritz-nullspace (Sec. 4.2) and by the Lagrange multipliers (Sec. 4.1) approaches. Thus, the Rayleigh-Ritz-nullspace approcah is utilized in the following examples, as it is computationally more efficient.

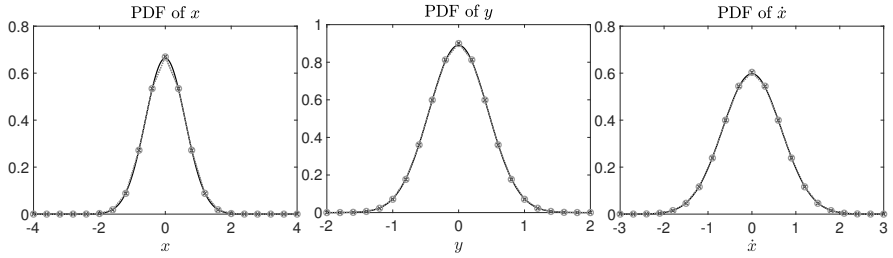

(a) displacement x (b) electrical quantity y (c) velocity $\dot{x}$

Figure 1: Stationary marginal response PDFs of a linear energy harvester with $\zeta = 0.1$, $\kappa = 0.65$, $\alpha = 0.8$, $\delta = 0$ and $S_0 = 0.05$. **Solid black line:** Gaussian PDF - Exact solution **Dotted line with "x":** WPI Rayleigh-Ritz-nullspace approach with 7 Legendre polynomials, **Dotted line with "o":** WPI E-L equations - Lagrange multipliers approach.

For the chosen value of the electrical constant ($\alpha = 0.8$), which is neither too small ($\to 0$), nor too large ($\to \infty$), it is anticipated by observing Eq. (1b), that the response of the electrical quantity y is correlated with both the mechanical displacement x and velocity $\dot{x}$, as discussed in Sec. 2. Indeed, this is depicted in the joint PDFs $p(y, x)$ and $p(y, \dot{x})$, shown in figures 2a and 2b, respectively.

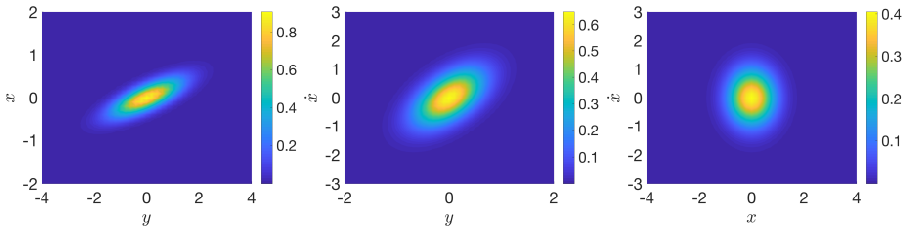

(a) $p(y, x)$ (b) $p(y, \dot{x})$ (c) $p(x, \dot{x})$

Figure 2: Stationary joint response PDFs of a linear energy harvester with $\zeta = 0.1$, $\kappa = 0.65$, $\alpha = 0.8$, $\delta = 0$ and $S_0 = 0.05$ determined by the WPI Rayleigh-Ritz-nullspace approach with 7 Legendre polynomials.

Further, as the value of α increases, y is expected to become more correlated with $\dot{x}$ and less correlated with x (see Eq. (1b)). Indeed, this is depicted in figures 3a and 3b, where the stationary joint response PDFs $p(y, x)$ and $p(y, \dot{x})$ are shown, respectively, for the energy harvester with the same parameters as in Fig. 2, but with a larger electrical constant $\alpha = 3$.

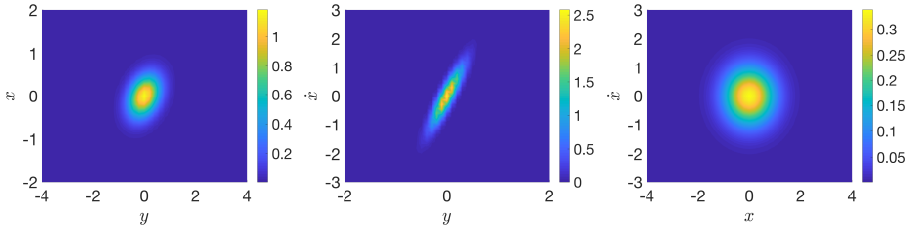

(a) $p(y, x)$ (b) $p(y, \dot{x})$ (c) $p(x, \dot{x})$

Figure 3: Stationary joint response PDFs of a linear energy harvester with $\zeta = 0.1$, $\kappa = 0.65$, $\alpha = 3.0$, $\delta = 0$ and $S_0 = 0.05$ determined by the WPI Rayleigh-Ritz-nullspace approach with 7 Legendre polynomials.

5.1.2. Nonlinear system

The nonlinear energy harvester with mono-stable asymmetric potential and parameters $\zeta = 0.1$, $\kappa = 0.65$, $\alpha = 0.8$, $\delta = 0.2$ and $S_0 = 0.05$ is considered next. The marginal stationary response PDFs of this energy harvester are shown in Fig. 4, where the WPI based solutions are compared both with

pertinent MCS data, and with solutions obtained by applying the statistical linearization method [20]. Clearly, because of the fundamental assumption of a Gaussian response PDF, a standard statistical linearization treatment fails to capture, not only the tails, but also basic features of the response PDFs. Indeed, considering the response PDF of x in Fig. 4a, it is seen that while the WPI technique exhibits a high degree of accuracy, the statistical linearization fails to capture the asymmetric shape due to the x^2 term in the nonlinear restoring force of Eq. (2). Note that this inadequacy of statistical linearization becomes significant from an optimization perspective as well, especially when a constrained optimization problem such as the one in Eq. (5) is considered. In particular, if maximizing $\mathbb{E}\{y^2\}$ is the only objective to be taken into account as in Eq. (4), then statistical linearization could potentially provide with relatively accurate results as suggested by the accuracy degree shown in Fig. 4b related to the PDF of y. However, if a more sophisticated optimization strategy is sought for, such as the one in Eq. (5) with a constraint of the form $P_f = P(|x| > x_{limit}) < \epsilon$, then satisfactory accuracy in estimating the tails of the PDF of x is obviously required. As clearly shown in Fig. 4a, this is achieved by the WPI technique, but not by a statistical linearization treatment.

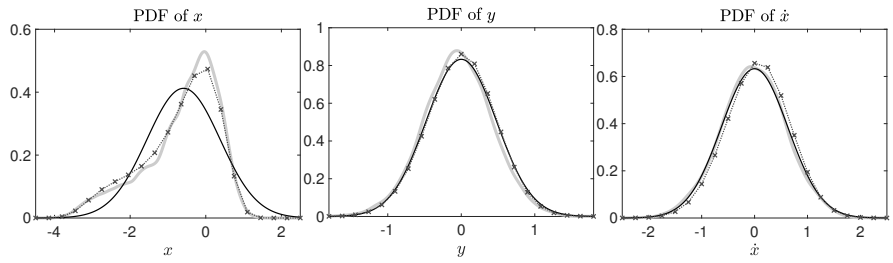

(a) displacement x (b) electrical quantity y (c) velocity $\dot{x}$

Figure 4: Stationary marginal response PDFs of a nonlinear energy harvester with $\zeta = 0.1$, $\kappa = 0.65$, $\alpha = 0.8$, $\delta = 0.2$ and $S_0 = 0.05$. **Solid gray line:** MC - 10000 realizations, **Solid black line:** Statistical linearization, **Dotted line with "x":** WPI Rayleigh-Ritz-nullspace approach with 7 Legendre polynomials.

Further, the significant effect of nonlinearities on the stationary joint re-

sponse PDFs can be readily seen by comparing Fig. 5 with Fig. 2.

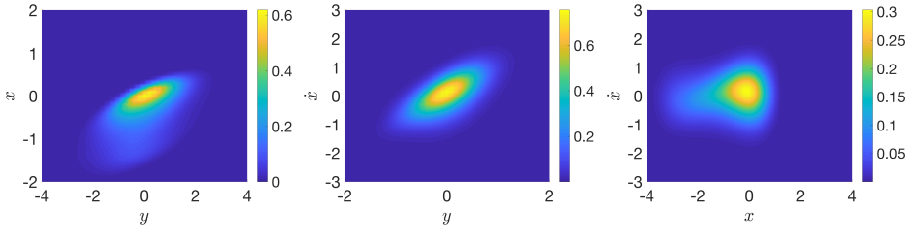

(a) $p(y, x)$ (b) $p(y, \dot{x})$ (c) $p(x, \dot{x})$

Figure 5: Stationary joint response PDFs of a nonlinear energy harvester with $\zeta = 0.1$, $\kappa = 0.65$, $\alpha = 0.8$, $\delta = 0.2$ and $S_0 = 0.05$ obtained by the WPI Rayleigh-Ritz-nullspace approach with 7 Legendre polynomials.

5.2. Energy harvester optimization with constraints

The constrained optimization problem of Eq. (5) is considered in this section. For this problem, the objective function $P_h(\boldsymbol{z})$ with $\boldsymbol{z} = [\alpha, \delta]^T$ is Eq. (3); thus, a procedure for calculating $\mathbb{E}\{y^2\}$ is required. Additionally, accounting for the constraint that the probability of failure does not exceed a prescribed threshold ϵ, requires knowledge of the joint response PDF. In this regard, the extended WPI technique developed in Sec. 4 in conjunction with the Rayleigh-Ritz-nullspace approach of Sec. 4.2 is employed next. Comparisons with a statistical linearization treatment are included as well, demonstrating the limitations and incapability of statistical linearization to handle constraints related to low probability events, as anticipated by examining Fig. 4a.

Two failure scenarios $x < x_{limit}$ and $|x| > x_{limit}$ are considered, and the corresponding probabilities of failure are defined as

$$P_f = P(x < x_{limit}) = \int_{-\infty}^{x_{limit}} p_s(x)\mathrm{d}x \tag{31}$$

$$P_f = P(|x| > x_{limit}) = \int_{-\infty}^{-x_{limit}} p_s(x)\mathrm{d}x + \int_{x_{limit}}^{\infty} p_s(x)\mathrm{d}x \tag{32}$$

respectively, where $p_s(x)$ is the stationary marginal PDF of the mechanical displacement x. For the solution of the corresponding constrained optimization

problem (see Eq. (5)), a penalty approach is utilized. This yields an unconstrained problem with the modified objective function $P_{h,\epsilon}(\boldsymbol{z}) = \mathbb{1}_\epsilon(\boldsymbol{z})P_h(\boldsymbol{z})$ where $\boldsymbol{z} = [\alpha, \delta]^T$ and $\mathbb{1}_\epsilon$ is an indicator function defined as

$$\mathbb{1}_\epsilon(\boldsymbol{z}) = \begin{cases} 0, & P_f(\boldsymbol{z}) \geq \epsilon \\ 1, & \text{otherwise} \end{cases} \tag{33}$$

Taking into account that information regarding the gradient of $P_{h,\epsilon}(\boldsymbol{z})$ is not available in general, the gradient-free Generalized Pattern Search (GPS) optimization algorithm is utilized next [49]. It is noted that the GPS algorithm was further extended in [50] to account for bound constraints, while no assumptions about the differentiability and continuity of the objective function are required [51].

First, the performance of the GPS algorithm is assessed by comparisons with brute-force full grid evaluations of the objective function $P_{h,\epsilon}(\boldsymbol{z})$ by relying on statistical linearization. In this regard, a full grid computation of $P_{h,\epsilon}^{SL}(\alpha, \delta)$ in the interval $\{\alpha, \delta\} \subset [0.5, 1.5] \times [0, 0.5]$ with a mesh size of 0.007 and parameter values $\zeta = 0.1$, $\kappa = 0.65$ and $S_0 = 0.05$, is presented in Fig. 6, with the constraint $P_f = P(x < -3.0) \leq 10^{-2}$, showing the existence of a global optimum point.

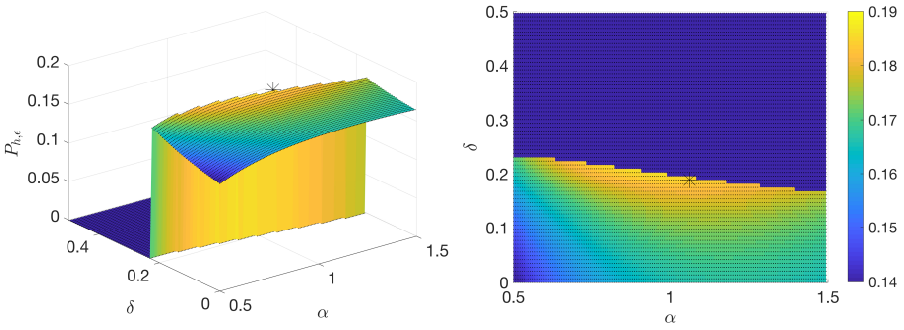

(a) 3D plot (b) overview plot

Figure 6: Stationary mean harvested power $P_{h,\epsilon}$ obtained by statistical linearization with constraint of the form of Eq. (31), and parameters $x_{limit} = -3.0$ and $\epsilon = 10^{-2}$. Full grid computation with mesh size 0.007 required 10296 objective function evaluations: $(\alpha_{opt}, \delta_{opt}) = (1.0600, 0.1890)$, $P^{SL}_{h,\epsilon}(\alpha_{opt}, \delta_{opt}) = 0.1850$ and $P_f(\alpha_{opt}, \delta_{opt}) = 0.009864$.

It can be readily seen that multiplication with $\mathbb{1}_\epsilon$, introduces a discontinuity to the objective function. Convergence of the GPS algorithm, however, does not assume continuity [51], and thus, the algorithm is expected to exhibit satisfactory performance in this particular discontinuous optimization problem. To test the validity of the above argument, the GPS algorithm is employed to solve the same problem and the results presented in Fig. 7 exhibit practically the same accuracy as the full grid computation. Note, however, that approximately only $\sim 0.5\%$ of the objective function evaluations used in the full grid computation are required by the GPS algorithm, rendering the overall optimization scheme computationally efficient.

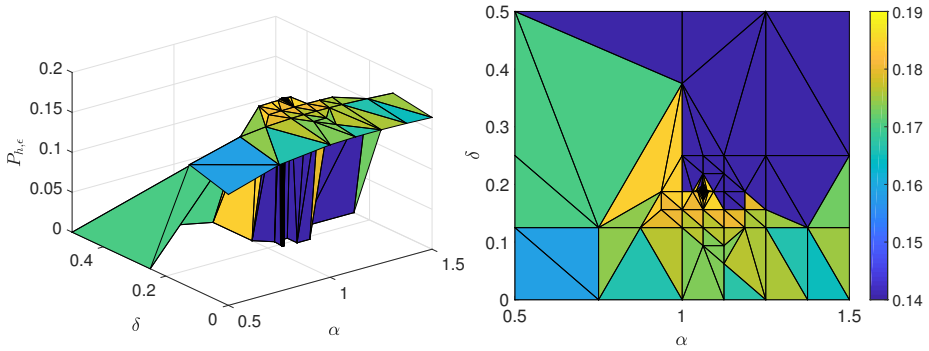

(a) 3D plot

(b) overview plot

Figure 7: Stationary mean harvested power $P_{h,\epsilon}$ obtained by statistical linearization with constraint of the form of Eq. (31), and parameters $x_{limit} = -3.0$ and $\epsilon = 10^{-2}$. GPS optimization required 164 objective function evaluations to converge: $(\alpha_{opt}, \delta_{opt}) = (1.0580, 0.1907)$, $P^{SL}_{h,\epsilon}(\alpha_{opt}, \delta_{opt}) = 0.1853$ and $P_f(\alpha_{opt}, \delta_{opt}) = 0.009987$.

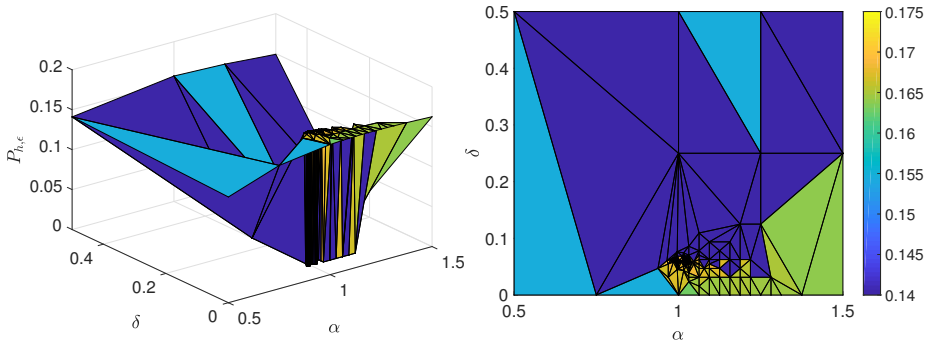

(a) 3D plot

(b) overview plot

Figure 8: Stationary mean harvested power $P_{h,\epsilon}$ obtained by WPI with constraint of the form of Eq. (31), and parameters $x_{limit} = -3.0$ and $\epsilon = 10^{-2}$. GPS optimization required 144 objective function evaluations to converge: $(\alpha_{opt}, \delta_{opt}) = (0.9874, 0.0625)$, $P^{WPI}_{h,\epsilon}(\alpha_{opt}, \delta_{opt}) = 0.1689$ and $P_f(\alpha_{opt}, \delta_{opt}) = 0.009981$.

315 Finally, the optimization results obtained by the WPI technique are shown in Fig. 8, revealing the significant but anticipated difference between the WPI and the linearization based optimal designs. This is attributed primarily to the incapability of statistical linearization to capture accurately the tails of the

Constraint: $P_f = P(x < -3.0) \leq 10^{-2}$		
	WPI optimum $(\alpha, \delta) = (0.9874, 0.0625)$	Stat. Lin. optimum $(\alpha, \delta) = (1.0580, 0.1907)$
P_h	0.16886	0.18530
P_f	0.00998	0.00999
MCS		
P_h	0.17021	0.17731
P_f	0.00932	0.03664

Table 1: Assessment of the WPI and statistical linearization based optima using MCS with 50000 realizations.

response PDF, which are related to the constraint of Eq. (31). The above argument is corroborated further by Table 1, where the WPI and linearization based optimal designs are assessed by using MCS. In particular, the WPI based optimum design yields a probability of failure of 0.00932, which is very close to the prescribed threshold (10^{-2}). On the other hand, the linearization based optimum yields a probability of failure $P_f = 0.03664$ that is significantly larger than 10^{-2}. Thus, the statistical linearization based optimal design violates the imposed constraint, rendering the technique unsuitable for handling low probability events.

Similar conclusions can be drawn if a more conservative failure event, e.g. $x < -2.0$ is considered. The optimal WPI and linearization based designs are shown in Table 2, where it is observed that the optimal δ values are reduced compared to the values in Table 1. As anticipated, this "stricter" constraint promotes a system behavior closer to linear. Similarly as in Table 1, MCS data in Table 2 based on the optimal designs demonstrate the relatively high accuracy degree of the WPI technique, as well as the inadequacy of statistical linearization to satisfy the imposed constraint.

As the nonlinearity magnitude δ increases, the asymmetry degree of the marginal PDF of x increases as well. Thus, the shapes of the left and the

Constraint: $P_f = P(x < -2.0) \leq 10^{-2}$		
	WPI optimum $(\alpha, \delta) = (1.1121, 0.0310)$	Stat. Lin. optimum $(\alpha, \delta) = (1.1220, 0.1002)$
P_h	0.16572	0.17411
P_f	0.00999	0.00999
MCS		
P_h	0.16926	0.17185
P_f	0.00996	0.07382

Table 2: Assessment of the WPI and statistical linearization based optima using MCS with 50000 realizations.

right PDF tails become substantially different (see Fig. 4a). For this reason, it is expected that statistical linearization, which assumes a symmetric Gaussian response PDF, will perform poorly in cases of constraints of Eq. (32) referring to both tails of the PDF. Indeed, for $x_{limit} = 2.0$ in Eq. (32), the corresponding WPI and statistical linearization based optimal designs are assessed by using MCS and the results are shown in Table 3. It is observed, that due to the relatively "steep" right tail of the PDF of x, the WPI optimum designs for the failure events $x < -2.0$ and $|x| > 2.0$ are identical, i.e. the probability $P(x > 2.0)$ is zero. In the statistical linearization based optimization, however, the two failure events lead to slightly different designs because the Gaussian response PDF of x is not steep enough at the right tail leading to $P(x > 2.0) > 0$. In a similar manner as in the previous examples, the statistical linearization based optimal design violates again the imposed constraint.

6. Concluding remarks

A methodology based on the WPI technique has been developed for determining the response of a class of nonlinear electromechanical energy harvesters subject to Gaussian white noise excitation. In this regard, the WPI technique [23–25] has been extended herein to account for a singular diffusion matrix

Constraint: $P_f = P(\|x\| > 2.0) \leq 10^{-2}$		
	WPI optimum $(\alpha, \delta) = (1.1121, 0.0310)$	Stat. Lin. optimum $(\alpha, \delta) = (1.1244, 0.0969)$
P_h	0.16572	0.17382
P_f	0.00999	0.00999
MCS		
P_h	0.16926	0.17114
P_f	0.00996	0.07072

Table 3: Assessment of the WPI and statistical linearization based optima using MCS with 50000 realizations.

present in the governing equations. Specifically, treating the coupled electromechanical equations as an "underdetermined" SDE in conjunction with a constraint equation has yielded a constrained variational problem. This has been solved either via a Lagrange multipliers approach, or by utilizing the nullspace of the constraint equation. It has been shown that the WPI technique exhibits satisfactory accuracy in determining the joint response PDF as compared with pertinent MCS data, and significantly outperforms an alternative statistical linearization treatment. Indeed, the inadequacy of statistical linearization in capturing even the basic features of the response PDF becomes more prevalent in nonlinear harvesters with asymmetric potentials, where the response PDF deviates significantly from the Gaussian.

Next, the herein extended WPI technique has been coupled with an appropriate optimization algorithm for determining optimal parameters for the energy harvester. In particular, a GPS algorithm [51] has been employed, and has been shown to converge to the global optimum even for the case of a discontinuous objective function. This appears when a constrained optimization problem is considered with constraints referring to probabilities of failure. For such cases, where relatively high accuracy in determining the response PDF tails is required, optimization based on statistical linearization yields, in general, either

sub-optimal solutions or solutions that violate the constraint.

Acknowledgments

I. A. Kougioumtzoglou gratefully acknowledges the support through his CAREER award by the CMMI Division of the National Science Foundation, USA (Award number: 1748537).

References

[1] H. A. Sodano, D. J. Inman, G. Park, A review of power harvesting from vibration using piezoelectric materials, Shock and Vibration Digest 36 (3) (2004) 197–206.

[2] H. A. Sodano, D. J. Inman, G. Park, Generation and storage of electricity from power harvesting devices, Journal of Intelligent material systems and structures 16 (1) (2005) 67–75.

[3] M. F. Daqaq, R. Masana, A. Erturk, D. D. Quinn, On the role of nonlinearities in vibratory energy harvesting: a critical review and discussion, Applied Mechanics Reviews 66 (4) (2014) 040801.

[4] N. G. Elvin, N. Lajnef, A. A. Elvin, Feasibility of structural monitoring with vibration powered sensors, Smart materials and structures 15 (4) (2006) 977.

[5] T. Galchev, J. McCullagh, R. Peterson, K. Najafi, Harvesting traffic-induced vibrations for structural health monitoring of bridges, Journal of Micromechanics and Microengineering 21 (10) (2011) 104005.

[6] M. Amin Karami, D. J. Inman, Powering pacemakers from heartbeat vibrations using linear and nonlinear energy harvesters, Applied Physics Letters 100 (4) (2012) 042901.

[7] W.-J. Wu, Y.-Y. Chen, B.-S. Lee, J.-J. He, Y.-T. Peng, Tunable resonant frequency power harvesting devices, in: Smart Structures and Materials 2006: Damping and Isolation, Vol. 6169, International Society for Optics and Photonics, 2006, p. 61690A.

[8] S. Shahruz, Limits of performance of mechanical band-pass filters used in energy scavenging, Journal of Sound and Vibration 293 (1-2) (2006) 449–461.

[9] B. Mann, N. Sims, Energy harvesting from the nonlinear oscillations of magnetic levitation, Journal of Sound and Vibration 319 (1-2) (2009) 515–530.

[10] L. Gammaitoni, I. Neri, H. Vocca, Nonlinear oscillators for vibration energy harvesting, Applied Physics Letters 94 (16) (2009) 164102.

[11] S. Adhikari, M. Friswell, D. Inman, Piezoelectric energy harvesting from broadband random vibrations, Smart Materials and Structures 18 (11) (2009) 115005.

[12] D. A. Barton, S. G. Burrow, L. R. Clare, Energy harvesting from vibrations with a nonlinear oscillator, Journal of Vibration and Acoustics 132 (2) (2010) 021009.

[13] M. F. Daqaq, Transduction of a bistable inductive generator driven by white and exponentially correlated gaussian noise, Journal of Sound and Vibration 330 (11) (2011) 2554–2564.

[14] H. Yoon, B. D. Youn, Stochastic quantification of the electric power generated by a piezoelectric energy harvester using a time–frequency analysis under non-stationary random vibrations, Smart Materials and Structures 23 (4) (2014) 045035.

[15] A. Erturk, D. J. Inman, Piezoelectric energy harvesting, John Wiley & Sons, New Jersey, 2011.

[16] G. Litak, M. Friswell, S. Adhikari, Magnetopiezoelastic energy harvesting driven by random excitations, Applied Physics Letters 96 (21) (2010) 214103.

[17] M. F. Daqaq, Response of uni-modal duffing-type harvesters to random forced excitations, Journal of Sound and Vibration 329 (18) (2010) 3621–3631.

[18] P. Green, K. Worden, K. Atallah, N. Sims, The benefits of duffing-type nonlinearities and electrical optimisation of a mono-stable energy harvester under white gaussian excitations, Journal of Sound and Vibration 331 (20) (2012) 4504–4517.

[19] S. Adhikari, M. Friswell, G. Litak, H. H. Khodaparast, Design and analysis of vibration energy harvesters based on peak response statistics, Smart Materials and Structures 25 (6) (2016) 065009.

[20] J. B. Roberts, P. D. Spanos, Random Vibration and Statistical Linearization (Dover Civil and Mechanical Engineering), Dover Publications, Mineola, NY, 2003.

[21] Q. He, M. F. Daqaq, Electric load optimization of a nonlinear mono-stable duffing harvester excited by white noise, Meccanica 51 (5) (2016) 1027–1039.

[22] S. Ali, S. Adhikari, M. Friswell, S. Narayanan, The analysis of piezomagnetoelastic energy harvesters under broadband random excitations, Journal of Applied Physics 109 (7) (2011) 074904.

[23] I. Kougioumtzoglou, P. Spanos, An analytical Wiener path integral technique for non-stationary response determination of nonlinear oscillators, Probabilistic Engineering Mechanics 28 (2012) 125–131.

[24] I. A. Kougioumtzoglou, P. D. Spanos, Nonstationary stochastic response determination of nonlinear systems: A Wiener path integral formalism, Journal of Engineering Mechanics 140 (9) (2014) 04014064.

[25] I. A. Kougioumtzoglou, A. Di Matteo, P. D. Spanos, A. Pirrotta, M. Di Paola, An efficient Wiener path integral technique formulation for stochastic response determination of nonlinear mdof systems, Journal of Applied Mechanics 82 (10) (2015) 101005.

[26] I. A. Kougioumtzoglou, A Wiener Path Integral Solution Treatment and Effective Material Properties of a Class of One-Dimensional Stochastic Mechanics Problems, Journal of Engineering Mechanics 143 (6) (2017) 04017014.

[27] A. Di Matteo, I. A. Kougioumtzoglou, A. Pirrotta, P. D. Spanos, M. Di Paola, Stochastic response determination of nonlinear oscillators with fractional derivatives elements via the Wiener Path Integral, Probabilistic Engineering Mechanics 38 (2014) 127–135.

[28] B. van Brunt, The Calculus of Variations (Universitext), Springer, New York, 2003.

[29] J. Nocedal, S. Wright, Numerical Optimization (Springer Series in Operations Research and Financial Engineering), Springer, New York, 2006.

[30] R. Harne, K. Wang, A review of the recent research on vibration energy harvesting via bistable systems, Smart materials and structures 22 (2) (2013) 023001.

[31] H. K. Joo, T. P. Sapsis, Performance measures for single-degree-of-freedom energy harvesters under stochastic excitation, Journal of Sound and Vibration 333 (19) (2014) 4695–4710.

[32] E. Halvorsen, Fundamental issues in nonlinear wideband-vibration energy harvesting, Physical Review E 87 (4) (2013) 042129.

[33] R. Langley, A general mass law for broadband energy harvesting, Journal of Sound and Vibration 333 (3) (2014) 927–936.

[34] R. S. Langley, Bounds on the vibrational energy that can be harvested from random base motion, Journal of Sound and Vibration 339 (2015) 247–261.

[35] Q. He, M. F. Daqaq, New insights into utilizing bistability for energy harvesting under white noise, Journal of Vibration and Acoustics 137 (2) (2015) 021009.

[36] M. Chaichian, A. Demichev, Path Integrals in Physics: Stochastic Processes and Quantum Mechanics, Institute of Physics Publishing, Bristol, U.K., 2001.

[37] G. M. Ewing, Calculus of Variations with Applications, Dover, New York, 1985.

[38] L. D. Elsgolc, Calculus of variations, Dover Publications, Mineola, N.Y, 2007.

[39] A. T. Meimaris, I. A. Kougioumtzoglou, A. A. Pantelous, A closed form approximation and error quantification for the response transition probability density function of a class of stochastic differential equations, Probabilistic Engineering Mechanics (2017) doi:http://dx.doi.org/10.1016/j.probengmech.2017.07.005.

[40] O. C. Zienkiewicz, Finite elements and approximation, Dover Publications, Mineola, N.Y, 2006.

[41] H. Rund, Hamilton Jacobi Theory in the Calculus of Variations Its Role in Mathematics Theory and Application, Krieger Pub Co, London, 1973.

[42] C. Lanczos, The Variational Principles of Mechanics (Dover Books on Physics), Dover Publications, Mineola, NY, 1986.

[43] M. Giaquinta, S. Hildebrandt, Calculus of Variations I (Grundlehren der mathematischen Wissenschaften) (Vol 1), Springer, Berlin, 2006.

[44] G. Oriolo, Y. Nakamura, Control of mechanical systems with second-order nonholonomic constraints: Underactuated manipulators, in: Decision and

Control, 1991., Proceedings of the 30th IEEE Conference on, IEEE, 1991, pp. 2398–2403.

[45] C. Carathéodory, Calculus of Variations and Partial Differential Equations of First Order, American Mathematical Society, Rhode Island, 1999.

[46] G. Strang, Linear Algebra and Its Applications, 4th Edition, Thomson Higher Education, Belmont, CA, 2006.

[47] G. E. Shilov, Linear Algebra (Dover Books on Mathematics), Dover Publications, Mineola, NY, 1977.

[48] E. N. Antoniou, A. A. Pantelous, I. A. Kougioumtzoglou, A. Pirrotta, Response determination of linear dynamical systems with singular matrices: A polynomial matrix theory approach, Applied Mathematical Modelling 42 (2017) 423–440.

[49] V. Torczon, On the convergence of pattern search algorithms, SIAM Journal on optimization 7 (1) (1997) 1–25.

[50] R. M. Lewis, V. Torczon, Pattern search algorithms for bound constrained minimization, SIAM Journal on Optimization 9 (4) (1999) 1082–1099.

[51] C. Audet, J. E. Dennis Jr, Analysis of generalized pattern searches, SIAM Journal on optimization 13 (3) (2002) 889–903.